Transmedia transmission enhancement based on transformation acoustics

Yu-Ze Tian,[1] Rui Li,[1] Yan-Feng Wang,[1,2,*] Vincent Laude,[3] and Yue-Sheng Wang[1,4]

[1] *School of Mechanical Engineering, Tianjin University, 300350 Tianjin, China*
[2] *National Key Laboratory of Vehicle Power System, 300350 Tianjin, China*
[3] *Université de Franche-Comté, CNRS, Institut FEMTO-ST, F-25000 Besançon, France*
[4] *Institute of Engineering Mechanics, Beijing Jiaotong University, Beijing 100044, China*

Transmission enhancement of sound waves across the interface between media with different impedances is a classical problem in acoustic communication, for instance in the case of the water-air interface. Different strategies, including bubble-embedded metasurfaces or impedance-matched metamaterials, have been developed to render the interface transparent. Transmedia wave enhancement is up to now either broadband or incorporating customized wavefront manipulation. In this work, we explore the use of transformation acoustics and gauge transformation to realize both goals simultaneously. Transformation acoustics is first argued to provide lossless transmedia sound enhancement, though at the expense of adapting the cross-section to respect power-flow conservation. It is specifically proven that a gradient anisotropic metamaterial provides perfect transmission between two media in 2 dimensions and that perfect steering of sound waves is allowed as well. Gauge transformation theory is then adapted from transformation elasticity to provide 1-dimensional perfect sound transmission via a gradient Willis-like acoustic metamaterial. Finally, the two transformations are combined together to implement broadband acoustic transmission perfectly and focusing at the water-air interface. The lens designed by the proposed method is achromatic. The work in this paper is expected to provide alternative solutions for transmedia communication and to open new application scenarios for transformation acoustics.

Keywords: Transformation acoustics, Acoustic metamaterials, Transmedia transmission, Precise wave manipulation

I. INTRODUCTION

The enhancement of sound wave transmission through the water-air interface is receiving increasing attention[1], for applications to environmental monitoring and marine communications[2,3]. As a typical problem in wave propagation, it is well known that the transmitted power is related to the ratio of the acoustic impedances of the two media. Acoustic impedance, the product of sound speed and mass density, is thus generally used to describe the ability of homogeneous media to carry plane waves. At first sight, it seems impossible to transmit waves integrally between water and air[4]. There is indeed a huge contrast in acoustic impedance, of about 3600, which leads to a theoretical power transmission rate as low as 0.1%[5].

Two techniques have been developed along the past two decades to improve transmission: bubble scattering and transmission line theory. The potential of bubble scattering was first discovered in the analysis of the radiation characteristics of underwater point sound sources by Oleg[6–8]. It was predicted that natural sound sources, e.g. air bubbles oscillating under water, should be beneficial for transmedia sound transmission. This idea was then proven through multiple scattering theory and demonstrated experimentally by Bretagne et al.[9] with a meta-screen consisting of a single layer of bubbles. The bubble-embedded structure made of hydrophobic materials proposed by Cai et al. suggested a more practicable method[10] within the concept of metamaterials[11] and metasurfaces[12]. Efficient transmission at different frequencies was achieved by adjusting the immersion depth of the structure. The technique was recently simplified by Gong et al.[13] with membrane-sealing bubbles supplying better operability. Such designs can also be extended to multiple frequencies or be made broadband using series and parallel connected bubbles of different scales[14] or resonance modes[15].

Based on transmission line theory, another solution was proposed by Zhang et al.[16]. Non-reflective transmission can be observed when two mismatched media are connected through a composite waveguide with specific effective impedance. Similarly, Bok et al.[17] proposed a membrane-mass metasurface with extremely thin thickness and verified it experimentally. Interestingly, some bubble-based structures have also been found to provide matched equivalent impedance[10,14,15]. They however suffer from some critical limitations. Structures containing resonant components often lead to a relatively narrow operation bandwidth. Consequently, the efficiency and the information capacity of transmedia acoustic communications are difficult to improve. One may turn to focused vortex-based communication[18] to achieve multiplexing[19] at a given frequency. But the transmitted phase difference is then fixed in a discrete fashion to either $\pi/2$ or $3\pi/2$, as determined by transmission line theory[20]. This results in a huge obstacle for further modulation of the wave field, whereas custom phase modulation is essential.

Some solutions have been proposed to solve these issues. First, a wider operation bandwidth can be achieved by considering materials with gradient impedance distribution[21]. Direct water-air communication through acoustic wave was hence demonstrated by Zhou et al. with extremely high

capacity and accuracy[22]. But the relationship between gradient function and transmittance is not yet proven clearly[23]. Second, an arbitrary phase difference modulation can be supplied by the series connection of two or more different impedance-matched units for further enhancement and wavefront manipulation[24,25]. Additional functions like acoustic focusing enhancement and acoustic vortex generation were thus implemented. However, there is up to now no clear solution to simultaneously achieve both goals.

Transformation acoustics may offer an alternative solution[26,27]. It originates from coordinate transformation theory and enables many functionalities in electromagnetism[28,29], acoustics[30–34], elasticity[35–38], thermology[39–41], and even multi-coupled physics[42–44], due to the universal existence of coordinate transformation invariance in the governing equations[45]. Invisibility cloaking is the most commonly considered application[46]. The use of transformation theory for metasurface design has also aroused great interest[47,48]. Precise wave manipulation can be achieved by structures with specific gradients of properties. Furthermore, additional degrees of freedom become available for field regulation as the amplitude becomes adjustable with the introduction of gauge transformation[37,44,49]. However, most studies involving gauge transformations remain in transformation elasticity. It still has considerable potential in transformation acoustics.

In this paper, broadband transmedia sound transmission and enhancement is considered based on the combination of transformation acoustics and gauge transformation. It is first shown that two arbitrarily different media can be continuously connected using a 2D spatial transformation. Gauge transformation with a Willis-like material is then adapted from transformation elasticity and perfect acoustic transmission is realized in 1D. Finally, it is argued that phase modulation can be allowed when combining the two transformations together. As an example, a broadband and achromatic lens is designed for acoustic signal enhancement. All theoretical developments are validated through numerical simulation.

II. METAMATERIAL DESIGN BASED ON THE INVERSE ANALYSIS OF TRANSFORMATION ACOUSTICS

Transformation theory originates from the coordinate transformation method. The solving process can be interpreted as applying a mapping $\mathcal{F}$ to the governing equation in original space, as shown in Fig. 1(a). The governing equation in transformed space is often described by curvilinear coordinates in a concise form. In the transformation, the original space with a regular grid is regarded as real or objective, whereas the transformed space is virtual.

The application of transformation theory to metamaterial design follows an inverse application of the coordinate transformation method, which is depicted in Fig. 1(b). A simple equation in virtual space with a known solution is considered first. The mapping $\mathcal{F}$ is then constructed to relate both coordinate systems. The coefficients of the transformed governing equation in real space, rather than the solution itself, serve as the major guidance during metamaterial design; they form the transformed material parameters. One can directly obtain the material parameters at given coordinates, as the grid is regular.

In the formulation of the transmedia problem we consider in this work, transformation theory is also applied inversely, as depicted in Fig. 1(c). There is however a crucial question that needs to be answered beforehand: which media can be connected together through a transformation? The question of the existence of a solution achieving simultaneously broadband transmission enhancement and arbitrary wavefront manipulation is indeed important but easily overlooked. Therefore, the mapping $\mathcal{F}$ should be checked first to connect different media. Appling it in the original space, the required parameters in the transformed space, i.e. the real space, can then be obtained.

Transformation theory in this paper is discussed along the following line. The original virtual space is occupied by the single material m_1 that is divided into three regions, as shown in Fig. 2. Three sub-mappings are applied to these three regions, respectively. Mapping $\mathcal{F}_1$ connects region m_1 on the left side to region m_1' in real transformed space. For simplicity, it is set as the identity mapping, so that original and transformed parameters are the same. Mapping $\mathcal{F}_3$ connects the original medium m_1 on the right side onto region m_3'. Note that it is a constant mapping if m_3' is a homogeneous medium. After these two mappings are determined, mapping $\mathcal{F}_2$ is established by imposing continuity conditions on the boundaries Γ_1 and Γ_2 separating the three regions. m_2' is therefore a gradient metamaterial with spatially varying parameters. Theoretically, waves can propagate from m_1' to m_3' through m_2' without reflection, just like they would in a homogeneous medium.

A. 2D metamaterials based on transformation acoustics with spatial transformation

Under the framework of transformation acoustics, the original space is described by a scalar Helmholtz equation. The governing equation for time-harmonic acoustic waves in homogeneous medium with a mass density ρ and a bulk modulus

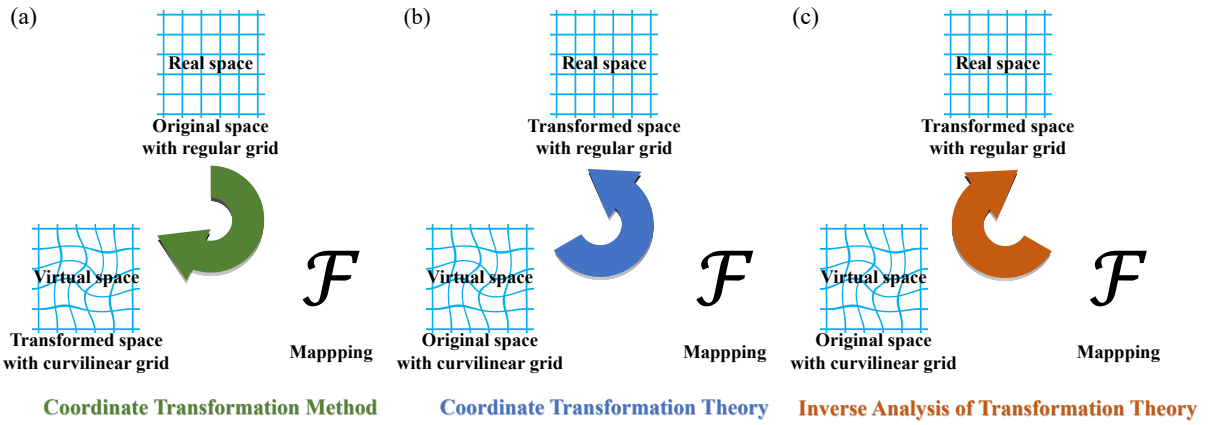

FIG. 1: Schematic diagram of (a) coordinate transformation method, (b) transformation theory, (c) inverse analysis of transformation theory.

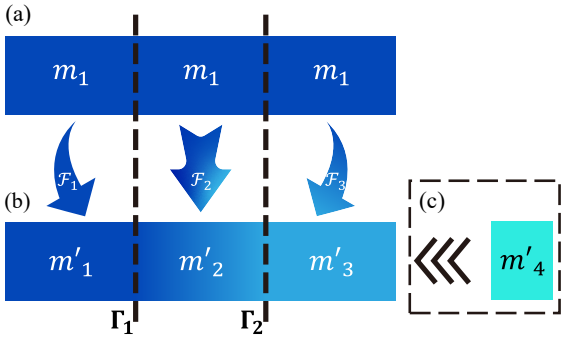

FIG. 2: Schematic diagram of transmedia problem based on transformation metamaterials. (a) The original space is occupied by material m_1 and divided into three regions. (b) The transformed space consist of three media m'_1, m'_2 and m'_3, and is obtained by three different transformations. The transformed space and the original space share consistent continuity at Γ_1 and Γ_2. (c) Replacing m'_3 with an impedance-matched medium m'_4, plane waves can be transmitted without reflection.

K then reads

$$\nabla \cdot \rho^{-1} \nabla p\left(\mathbf{x}\right) + \omega^2 K^{-1} p\left(\mathbf{x}\right) = 0, \tag{1}$$

where ω is the angular frequency and $\nabla = \frac{\partial}{\partial x}\mathbf{e}_x + \frac{\partial}{\partial y}\mathbf{e}_y$ is the gradient operator in original space. The mapping $\mathcal{F}$ is represented by the transformation matrix

$$F\left(\mathbf{x}'\right) = \frac{\partial \mathbf{x}'}{\partial \mathbf{x}} = \begin{bmatrix} \frac{\partial x'}{\partial x} & \frac{\partial x'}{\partial y} \\ \frac{\partial y'}{\partial x} & \frac{\partial y'}{\partial y} \end{bmatrix} \tag{2}$$

whose determinant is the Jacobian J. Substituting Eq. (2) into Eq. (1), the transformed governing equation is

$$\nabla' \cdot \left[\rho'^{-1}\left(\mathbf{x}'\right) \nabla' p\left(\mathbf{x}'\right)\right] + \omega^2 K'^{-1}\left(\mathbf{x}'\right) p\left(\mathbf{x}'\right) = 0, \tag{3}$$

where $\nabla' = \frac{\partial}{\partial x}\mathbf{e}_{x'} + \frac{\partial}{\partial y}\mathbf{e}_{y'}$ is the gradient operator in transformed space. The transformed specific volume is the tensor

$$\rho'^{-1}\left(\mathbf{x}'\right) = \rho^{-1}\frac{FF^T}{J} \tag{4}$$

and the transformed bulk modulus is the scalar

$$K'^{-1}\left(\mathbf{x}'\right) = \frac{K^{-1}}{J}. \tag{5}$$

The mapping $\mathcal{F}_3$ relates two homogeneous media so the restriction of the transformation matrix to region m'_3 is a constant matrix

$$F\left(\mathbf{x}'\right)|_{m'_3} = F_3 = \begin{bmatrix} a & b \\ c & d \end{bmatrix}. \tag{6}$$

Since we want m'_3 to be a natural material, for instance air, the specific volume is imposed to be isotropic

$$\rho'^{-1}\left(\mathbf{x}'\right)|_{m_3} = \rho^{-1}\frac{F_3 F_3^T}{J_3} = \rho'^{-1} I. \tag{7}$$

The ratios of mass densities and bulk moduli before and after transformation are respectively defined as $\alpha = \frac{\rho'}{\rho}$ and $\beta = \frac{K'}{K}$. Hence, the components of the transformation matrix obey the relations

$$\frac{a^2 + b^2}{ad - bc} = \alpha, \tag{8a}$$
$$ac + bd = 0, \tag{8b}$$
$$ad - bc = \beta, \tag{8c}$$
$$\frac{c^2 + d^2}{ad - bc} = \alpha. \tag{8d}$$

These equations have no solution if $\alpha \neq 1$, as shown in Appendix A. This condition imposes the transformation to act only on the bulk modulus but to leave the mass density unchanged. Setting

$\alpha = 1$ and writing $a = a_0$, the transformation matrix can be solved as

$$F_3 = \begin{bmatrix} a_0 & \pm\sqrt{\beta - a_0^2} \\ \mp\sqrt{\beta - a_0^2} & a_0 \end{bmatrix}. \tag{9}$$

Substituting into Eq. (2), the coordinate transformation is obtained by integration

$$\left\{ \begin{array}{lrll} x' = & a_0 x & \pm\sqrt{\beta - a_0^2}\, y & +h_x, \\ y' = & \mp\sqrt{\beta - a_0^2}\, x & +a_0 y & +h_y. \end{array} \right\} \tag{10}$$

where h_x and h_y are constants. It can be noted that $0 \leq |a_0| \leq \sqrt{\beta}$.

The polar decomposition of the transformation matrix $F_3 = VR$ ($RR^T = R^T R = I$, $\det R = 1$, $V^2 = F_3 F_3^T$) is introduced to check its physical significance

$$F_3 = VR = \begin{bmatrix} \sqrt{\beta} & 0 \\ 0 & \sqrt{\beta} \end{bmatrix} \begin{bmatrix} \sqrt{\frac{a_0^2}{\beta}} & \pm\sqrt{1 - \frac{a_0^2}{\beta}} \\ \mp\sqrt{1 - \frac{a_0^2}{\beta}} & \sqrt{\frac{a_0^2}{\beta}} \end{bmatrix}. \tag{11}$$

V is a stretching matrix that is uniquely determined by the ratio of bulk moduli. R is a rotation matrix. It can be noted that the ratio of the coefficients of the original coordinates in Eq. (10) determines the angle of rotation after transformation. There is no rotation only if $a_0^2 = \beta$.

We can now precise the mapping $\mathcal{F}_2$. Continuity conditions[44] need to be satisfied on boundaries Γ_1 and Γ_2

$$F_2(\mathbf{x}')|_{\Gamma_1} = F_1(\mathbf{x}')|_{\Gamma_1} = I, \tag{12}$$
$$F_2(\mathbf{x}')|_{\Gamma_2} = F_3(\mathbf{x}')|_{\Gamma_2} = F_3. \tag{13}$$

In between these boundaries, we request the mapping to vary smoothly with space coordinates, for instance as a polynomial of x and y, but it is not uniquely defined. A specific example with simple parameters is provided next as a intuitive demonstration of the design process for transformation metamaterials. The original space is set as a waveguide filled with water with a mass density of $\rho_w = 1000$ kg/m^3 and a bulk modulus of $K_w = 2.25 \times 10^9$ Pa. Assuming that the medium to be connected owns a mass density $\rho' = \rho_w$ and a bulk modulus $K' = K_w/4$, then $\alpha = 1$ and $\beta = 0.25$. Impedances are mismatched, with the impedance ratio $\gamma = \frac{Z'}{Z_w} = \sqrt{\alpha\beta} = 0.5$. The original space is composed of three rectangles with the same height $h_w = 10$ cm. The length of the left and right parts is set to $w_s = 50$ cm, whereas the length of the middle part is set to $w_m = 20$ cm. The origin of the coordinate system is chosen at the center of the middle part for convenience. A plane wave with unit amplitude is incident along the positive x direction. The line segment with endpoints $(-w_m/2, 0)$ and $(w_m/2, 0)$ is imposed to remain unchanged under transformation, so that

$$\mathcal{F}_2(\mathbf{x}, 0) = (\mathbf{x}', 0). \tag{14}$$

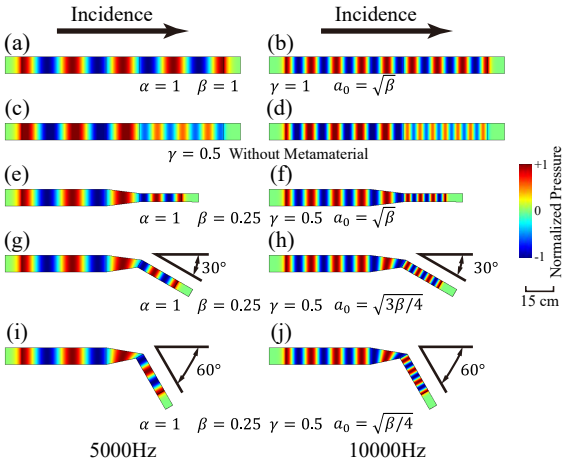

FIG. 3: Response for plane wave incidence under different configurations. The normalized pressure is shown in all panels. A homogeneous medium with $\alpha = 1, \beta = 1, \gamma = 1$ and $a_0 = \sqrt{\beta}$ is considered first at frequencies (a) $f_1 = 5000$ Hz and (b) $f_2 = 10000$ Hz. (c-d) Two impedance-mismatched media with $\gamma = 0.5$ are connected through a bare interface. Two impedance-mismatched media with $\alpha = 1, \beta = 0.25$ and $\gamma = 0.5$ are then connected by a metamaterial based on spatial transformation for (e-f) $a_{0,1} = \sqrt{\beta}$, (g-h) $a_{0,2} = \sqrt{3\beta/4}$, and(i-j) $a_{0,3} = \sqrt{\beta/4}$.

The transformation $\mathcal{F}_2$ and the constants h_x and h_y are obtained by inspection, combining Eqs. (12), (13) and (14), and considering the simplest possible polynomial dependence:

$$\left\{ \begin{array}{ll} x' = & x \pm \frac{\sqrt{\beta - a_0^2}}{2} y \pm \frac{\sqrt{\beta - a_0^2}}{w_m} xy, \\ y' = & \frac{a_0 + 1}{2} y - \frac{1 - a_0}{w_m} xy. \end{array} \right. \tag{15}$$

$$h_x = (1 - a_0)\, w_m, \tag{16}$$

$$h_y = \sqrt{\beta - a_0^2}\, w_m. \tag{17}$$

The analysis presented above is frequency independent, hence the results should be both broadband and achromatic. Two operating frequencies, $f_1 = 5000$ Hz and $f_2 = 10000$ Hz, are adopted in the following numerical simulations. The computation domain is terminated on both sides by two perfectly matched layers (PML) with a thickness of 10 cm, in order to avoid external reflections. Three cases are considered, with $a_0 = \sqrt{\beta}$, $\sqrt{3\beta/4}$ and $\sqrt{\beta/4}$. It can be inferred from the polar decomposition of the transformation matrix [Eq. (11)] that the positive or negative value of b in Eq. (9) determines the sign of the rotation angle. We set $b = +\sqrt{\beta - a_0^2}$ in the following discussion for convenience. Detailed metamaterial parameters are given in Appendix B. Simulation results are summarized in Fig. 3. The sound fields of Figs. 3(a-b) in the original space are shown for reference ($\alpha = \beta = \gamma = 1, a_0 = \sqrt{\beta}$). When $\gamma = 0.5$, there is impedance contrast at a planar interface leading to partial transmission of sound waves, as shown

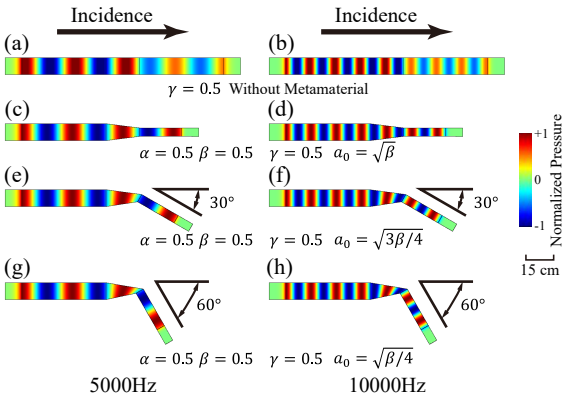

FIG. 4: Response for plane wave incidence under different configurations. The normalized pressure is shown in all panels. Two impedance-mismatched media with $\gamma = 0.5$ are connected through a bare interface are considered first at frequencies (a) $f_1 = 5000$ Hz and (b) $f_2 = 10000$ Hz. Two impedance-mismatched media with $\alpha = 0.5, \beta = 0.5$ and $\gamma = 0.5$ are then connected by a metamaterial based on spatial transformation for (c-d) $a_{0,1} = \sqrt{\beta}$, (e-f) $a_{0,2} = \sqrt{3\beta/4}$, and (g-h) $a_{0,3} = \sqrt{\beta/4}$.

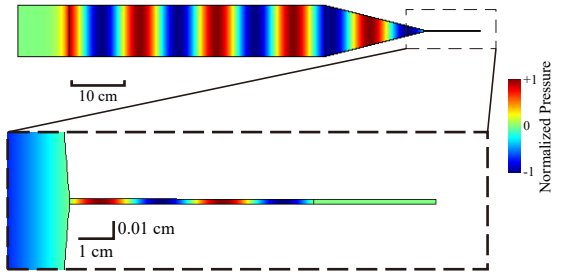

FIG. 5: The normalized pressure for a water-air transmedia metamaterial based on spatial transformation is shown at 10000 Hz. The huge contrast in impedance between water and air leads to small port areas on the air side.

in Figs. 3(c-d). The remaining panels show what happens when the metamaterial based on transformation acoustics is introduced, keeping $\gamma = 0.5$ constant. For $a_{0,1} = \sqrt{\beta}$, as shown in Figs. 3(e-f), the rotation angle is zero; the medium on the transmitted side narrows and shortens under the coordinate transform and the wavelength become shorter. The sound wave is perfectly transmitted into the target medium, maintaining a planar mode. The amplitude of the pressure in every section of the sound field is unitary, inside as swell as on both sides of the metamaterial. If a_0 is decreased, the transmitted wave is steered with a refraction angle $\theta = \arctan\sqrt{\frac{\beta}{a_0^2} - 1}$. For $a_{0,2} = \sqrt{3\beta/4}$, as shown in Figs. 3(g-h), the refraction angle is 30°. For $a_{0,3} = \sqrt{\beta/4}$, as shown in Figs. 3(i-j), the refraction angle is 60°. 100% transmission efficiency is obtained in all cases, regardless of the angle of rotation.

The condition $\alpha = 1$ is a strong limitation, since only media with the same mass density can be connected. Fortunately, the theory can be further developed in conjunction with impedance matching theory. A medium m_4' whose acoustic impedance is the same as that of m_3' can be connected onto it without causing any reflection. Further setting the thickness of m_3' to zero, the transmission medium is replaced directly with m_4', as shown Fig. 2(c). Transmission should still be perfect under the excitation of plane waves. Consider for concreteness a medium m_4' with mass density $\rho' = \rho_w/2$ and bulk modulus $K' = K_w/2$, so that $\alpha = 0.5$ and $\beta = 0.5$. The impedance ratio with m_1' is still $\gamma = 0.5$. The transmission between m_1' and m_4' remains partial when no metamaterial is introduced, as shown in Figs. 4(a-b). When the three metamaterials in Figs. 4(c-h), with $\alpha = 0.5, \beta = 0.5$ and $\gamma = 0.5$, are introduced as a connection perfect transmission can be observed again.

Theoretically, an impedance-matched connection between water and air can be achieved thanks to metamaterials based on spatial transformation. The norm-preserving nature of the solution ensures that the amplitude of transmitted sound waves are equal to the amplitude of incident waves, which is a significant enhancement of the sound pressure compared to the plane wave value 1/60[24]. Setting the material of m_4' as air with mass density $\rho_a = 1.18$ kg/m^3 and bulk modulus $K = 1.38\times10^5$ Pa, the result of numerical simulation at 10000 Hz is given in Fig. 5. The metamaterial works as expected, but the reduction in waveguide cross-section is obviously strong.

It should be noted that the method in this section could be extended to 3D but does not work in 1D. Indeed, in 1D the material parameters change as

$$\rho'^{-1}(x') = \rho^{-1}\frac{\partial x'}{\partial x}, \tag{18}$$

$$K'^{-1}(x') = \frac{K^{-1}}{\partial x'/\partial x}, \tag{19}$$

hence the impedance ratio $\left(\gamma = \sqrt{\alpha\beta}\right)$ is always 1. This conclusion can also be reached by checking the conservation of power flow. In 2D or 3D, this conservation expresses as

$$\frac{|p_1^2|}{2Z_1} \times A_1 = \frac{|p_2^2|}{2Z_2} \times A_2. \tag{20}$$

where A_1 and A_2 are the areas of the incident and transmission ports, respectively. Due to the norm-preserving nature of the spatial transformation ($p_1 = p_2$), a difference in impedance directly results in a change in port area, $\left(\frac{Z_1}{Z_2} = \frac{A_1}{A_2}\right)$. That characteristic can be observed in both Figs. 3 and

4. For the 1D case, in contrast, the ratio of port areas is always 1 and the impedance is unchanged in a 1D transformation.

B. 1D metamaterials based on transformation acoustics with gauge transformation

2D or 3D spatial transformation achieves perfect connection between arbitrary media, preserving the wave amplitude. The huge contrast in impedance between water and air, however, leads extremely small port areas on the air side, as apparent in Fig. 5. The ratio of port areas is $\frac{A_2}{A_1} = 1/60$. This fact makes the solution questionable in practice, despite the superior sound enhancement. Therefore, conventional transformation acoustics based on spatial transformation may only be suitable in case of slight impedance mismatch.

Gauge transformation, inspired by transformation elasticity[44], may provide an alternative solution. As an energy-preserving transformation, the wave amplitude becomes variable while the dispersion relation is not disturbed. It has been observed that Willis-like materials[50]are inevitably introduced by a gauge transformation[37,44,49]. Fortunately, there have been reports suggesting that materials with Willis-like properties are actually accessible[51,52] or can even be tunable[53]. The corresponding tuning strategies have also been thoroughly developed[54,55] for easier implementation. In this section, we examine how the Willis-like properties are introduced by transformation acoustics under a gauge transformation.

As a transformation on wave amplitude, 1D gauge transformation can be defined as

$$p\left(x\right) = G\left(x\right) p'\left(x\right). \tag{21}$$

Note that the spaces before and after transformation share the same regular coordinate system, which is a special case of Fig. 1(c). Substituting Eq. (21) into Eq. (1), the transformed governing equation is

$$\begin{aligned} &\frac{\partial}{\partial x}\left[\rho''^{-1}\left(x\right)\frac{\partial}{\partial x}p'\left(x\right) + S\left(x\right)p'\left(x\right)\right] \\ &= S\left(x\right)\frac{\partial}{\partial x}p'\left(x\right) + Ep'\left(x\right) - \omega^2 K''^{-1}\left(x\right)p'\left(x\right), \end{aligned} \tag{22}$$

where

$$\begin{cases} S(x) = \frac{G(x)}{\rho}\frac{\partial G(x)}{\partial x}, \\ E(x) = \frac{1}{\rho}\left(\frac{\partial G(x)}{\partial x}\right)^2, \end{cases} \tag{23}$$

are the Willis-like terms introduced by the gauge transformation. The transformed mass density and bulk modulus are

$$\rho''\left(x\right) = \frac{\rho}{G^2\left(x\right)}, \tag{24}$$

$$K''\left(x\right) = \frac{K}{G^2\left(x\right)}. \tag{25}$$

The acoustic impedance changes proportionally to $G^{-2}(x)$, as do $\rho(x)$ and $K(x)$. It can be noticed that Willis coupling requires a non constant gauge function $G(x)$, since parameters $S(x)$ and $E(x)$ are defined from its first derivative. When connecting different media, larger Willis coupling will result from larger impedance mismatch or thinner metamaterials.

As an important special case, we consider first a transformation between two homogeneous media, for which the gauge transformation should be linear. The Willis terms vanish and the parameters for the target material (m_3' in Fig. 2) are

$$\rho'' = \frac{\rho}{G_3^2}, \tag{26}$$

$$K'' = \frac{K}{G_3^2}, \tag{27}$$

with $\alpha = \beta = \gamma = G_3^{-2}$. As a note, the gauge transformation obeys the conservation of power flow, since

$$\frac{|p_1'^2|}{2Z_1} = \frac{G_3^2|p_2'^2|}{2Z_1} = \frac{|p_2'^2|}{2Z_2}. \tag{28}$$

Physically, the change in wave amplitude exactly compensates for the change in acoustic impedance, without impacting wave propagation.

Next, the gauge transformation for m_2' can be inferred to provide a smooth connection and is not unique. Here, we assume that the gauge transformation follows a polynomial form

$$G_2\left(x\right) = \sum_{i=0}^{n} a_i x^i. \tag{29}$$

The gauge transformation should be first-order differentiable on the boundaries $\Gamma_1 : x = x_1$ and $\Gamma_2 : x = x_2$, leading to the degradation condition[44]

$$G_2\left(x_1\right) = 1, \tag{30}$$

$$\frac{\partial G_2\left(x_1\right)}{\partial x} = 0, \tag{31}$$

$$G_2\left(x_2\right) = \gamma^{-\frac{1}{2}}, \tag{32}$$

$$\frac{\partial G_2\left(x_2\right)}{\partial x} = 0. \tag{33}$$

It can be checked by inspection that the simplest solution is obtained when $n = 3$ (there are no so-

lution for smaller polynomial degrees) and is

$$\begin{cases} a_3 = & \frac{2\left(\gamma^{-\frac{1}{2}}-1\right)}{(x_1-x_2)^3}, \\ a_2 = & \frac{-3(x_1+x_2)\left(\gamma^{-\frac{1}{2}}-1\right)}{(x_1-x_2)^3}, \\ a_1 = & \frac{6x_1x_2\left(\gamma^{-\frac{1}{2}}-1\right)}{(x_1-x_2)^3} \\ a_0 = & \frac{\gamma^{-\frac{1}{2}}x_1^3-3\gamma^{-\frac{1}{2}}x_1^2x_2+3x_1x_2^2-x_2^3}{(x_1-x_2)^3}. \end{cases} \tag{34}$$

Because gauge transformation affects the wave amplitude without touching spatial coordinates, the wavelength and the sound speed are unchanged. The impedance is modified, however, and connection between arbitrary media can be achieved by combining the solution with impedance matching theory, as illustrated in Fig. 2(c).

The water-air sound transmission using a metamaterial based on gauge transformation is considered now. The numerical simulation model adopts the same geometry settings as in the previous section. An intermediate medium m_3' with $\alpha = \beta = \gamma = \frac{Z_a}{Z_w}$ is used to establish the gauge transformation. Substituting these parameters, along with Eqs. (23-25,29,34), into Eq. (22), the results of numerical simulations are given in Figs. 6(a,b). Detailed metamaterial parameters are given in Appendix B.

Because of power flow conservation, the wave amplitude in region m_3' is relatively small. The transmitted wave has a normalized amplitude of about 1/60, which is exactly the theoretical limit value for complete transmission given by Eq. (28)[24]. The quantity $G(x)p'(x)$ is depicted in Figs. 6(c) and (d) for better observation. It can be noted that the results are actually consistent with the original field $p(x) = G(x)p'(x)$. The sound pressure distribution along axis $y = 0$ is shown in Fig. 6(e), together with the variations of $\pm\frac{1}{G(x)}$. It can be observed that the phase and wavelength remain unchanged after the gauge transformation. The envelope of the wave amplitude $|p'(x)|$ follows the gauge transformation $\pm\frac{1}{G(x)}$. Replacing region m_3' with region m_4' (air), the total fields $p'(x)$ and $G(x)p'(x)$ at operating frequencies f_1 and f_2 are given in Figs. 6(f-i). Intact sound transmission from water to air is achieved without reflection.

C. Transmedia acoustic lens based on spatial-gauge cooperative transformation

Although gauge transformation can achieve a perfect connection between arbitrary media in 1D and has the potential to be expanded to 2D or 3D, phase modulation is directly not included at first. However, it is essential in order to supply further wavefield modulation for transmedia acoustic communication. The combination of spatial and gauge transformations may provide a solution, as shown next, with 1D analysis as in the previous section.

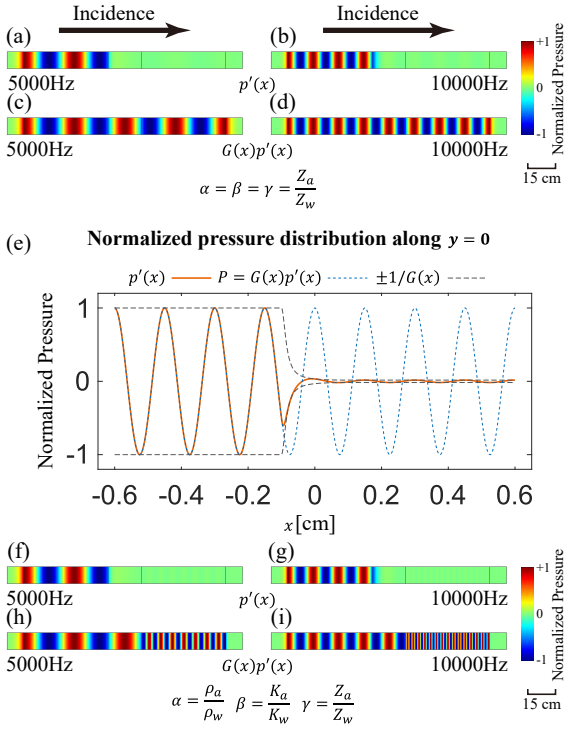

FIG. 6: Response for plane wave incidence under different configurations. The normalized pressure $p'(x)$ for two impedance-mismatched media connected by a metamaterial based on gauge transformation theory with $\alpha = \beta = \gamma = \frac{Z_a}{Z_w}$ is shown at frequencies (a) $f_1 = 5000$ Hz and (b) $f_2 = 10000$ Hz. (c-d) The gauge transformed pressure field $G(x)p'(x)$ has unitary amplitude variations. (e) The normalized pressure distributions $p(x)$ and $p'(x)$ are shown along $y = 0$, together with the gauge transformation function $\pm G(x)$. The normalized pressure $p'(x)$ for two impedance-mismatched media connected by a metamaterial based on gauge transformation theory with $\alpha = \frac{\rho_a}{\rho_w}$, $\beta = \frac{K_a}{K_w}$, and $\gamma = \frac{Z_a}{Z_w}$, is shown at frequencies (f) f_1 and (g) f_2. (h-i) The gauge transformed pressure field $G(x)p'(x)$ again has unitary amplitude variations.

The gauge transformation is now defined in transformed space as

$$p(x') = G(x')p'(x'). \tag{35}$$

Substituting Eq. (35) into Eq. (1), the transformed governing equation is given by

$$\frac{\partial}{\partial x'}\left[\rho'''^{-1}(x')\frac{\partial}{\partial x'}p'(x') + S'(x')p'(x')\right] = S'(x')\frac{\partial}{\partial x'}p'(x') + E'p'(x') - \omega^2 K'''^{-1}(x')p'(x'), \tag{36}$$

where

$$\begin{cases} S' = & \frac{G(x')}{\rho}\frac{\partial x'}{\partial x}\frac{\partial G(x')}{\partial x'}, \\ E' = & \frac{1}{\rho}\frac{\partial x'}{\partial x}\left(\frac{\partial G(x')}{\partial x}\right)^2, \end{cases} \tag{37}$$

are the Willis-like terms introduced by the spatial-gauge cooperative transformation. The transformed mass density and bulk modulus are

$$\rho'''(x') = \frac{\rho}{G^2(x')\frac{\partial x'}{\partial x}}, \tag{38}$$

$$K'''(x') = \frac{K}{G^2(x')}\frac{\partial x'}{\partial x}. \tag{39}$$

The acoustic impedance changes proportionally to $G^{-2}(x')$ and does not depend on the $\frac{\partial x'}{\partial x}$ term. In contrast, the acoustic velocity changes proportionally to $|\frac{\partial x'}{\partial x}|$ but does not depend on $G(x')$. Hence, the gauge transformation adapts the wave amplitude to the change in acoustic impedance, whereas the spatial transformation regulates the local wavelength.

For a transformation between two homogeneous media, the spatial-gauge cooperative transformation is linear

$$G(x')|_{m_3} = G_3 \tag{40}$$

$$x' = F_3 x + h_x \tag{41}$$

The Willis terms vanish, and the parameters for the target material (m_3 in Fig. 2) are

$$\rho'' = \frac{\rho}{G_3^2 F_3}, \tag{42}$$

$$K'' = \frac{K F_3}{G_3^2}. \tag{43}$$

The coefficients of the transformations can be solved uniquely as

$$G_3 = (\alpha\beta)^{-\frac{1}{4}} = \gamma^{-\frac{1}{2}}, \tag{44}$$

$$F_3 = (\beta/\alpha)^{\frac{1}{2}}. \tag{45}$$

It can be noted that the gauge transformation is only determined by the impedance ratio γ, which ensures the conservation of power flow expressed by Eq. (28). The spatial transformation is only determined by the ratio of sound speeds, $F_3 = \frac{c'}{c}$. Transformation between arbitrary media can thus be achieved considering these two independent design variables.

Transformation $\mathcal{F}_2$ is again determined by the continuity conditions [Eqs. (12-13)] and the degradation conditions [Eqs. (30-33)] as

$$x' = \frac{F_3 x_2 - x_1 + h_x}{x_2 - x_1}(x - x_1) + x_1 \tag{46}$$

$$F_2 = \frac{\partial x'}{\partial x} = \frac{F_3 x_2 - x_1 + h_x}{x_2 - x_1} \tag{47}$$

$$G_2(x') = a_0 + a_1 x' + a_2 x'^2 + a_3 x'^3. \tag{48}$$

For the given original coordinates x_1 and x_2, the length of the metamaterial changes with h_x according to

$$t = F_3 x_2 - x_1 + h_x. \tag{49}$$

Conversely, for fixed length $t = t_0$ and coordinate x_1, the phase difference can be adjusted by changing x_2. For different x_2 and $\hat{x_2}$, the phase difference at a given frequency f_0 is

$$\Delta\phi = k_0(x_2 - \hat{x_2}), \tag{50}$$

where k_0 is the wavenumber of the medium in original space. A metasurface based on generalized Snell's law can consequently be realized, for which phase modulation is achieved with perfect power flow conservation. An interesting fact is that when $x_1 = x_1'$ and $x_2 = x_2'$, the replacement from m_3' to m_4' is actually a linear transformation applied on m_3' along the propagation direction.

It appears from the theory of spatial-gauge transformation that perfect transmission can not be achieved with a graded material in 1D unless Willis coupling is added. Due to the degradation condition [Eqs. (30-33)], the gauge transformation has to be continuous at the boundaries. Willis coupling terms then arise naturally when writing the acoustic equation Eq. (37). They only vanish when $\gamma = 1$, which indicates that an impedance difference is not permitted at all without Willis coupling. In practice, considering the graded material described by Eqs. (38,39) only would provide a smooth connection between two impedance-mismatching media without involving Willis coupling. It is indeed generally considered intuitive that graded materials can provide transmittance with limited reflection. In order to precise this intuition, we provide an numerical simulation example in Appendix C that illustrates the contribution of Willis coupling to perfect transmission: in the absence of Willis coupling, large transmittance is achieved for high frequencies - or shorter wavelegnths - but strong reflection is observed for low frequencies - or longer wavelengths.

Transmedia manipulation of the wave field can now be implemented after phase difference modulation is allowed. Considering the decrease in amplitude from water to air, a focusing lens is designed at the interface for further enhancement of acoustic signals. Setting the center of the lens at $(0, 0)$ and the focal length to l_0, the distribution of phase difference along the y-axis is

$$\Delta\phi(y') = k_0'\left(\sqrt{y'^2 + l_0^2} - l_0\right) + C_0, \tag{51}$$

where k_0' is the wavenumber of the medium in transformed space at the operating frequency f_0. Substituting this expression into Eq. (50), $\hat{x_2}(y)$ should obey

$$\hat{x_2}(y') = \frac{k_0'}{k_0}\left(\sqrt{y'^2 + l_0^2} - l_0\right) + x_2 + C_0/k_0. \tag{52}$$

When the excitation frequency changes from f_0 to f_1, the wavenumbers in original space and transformation space become k_1 and k_1', respectively.

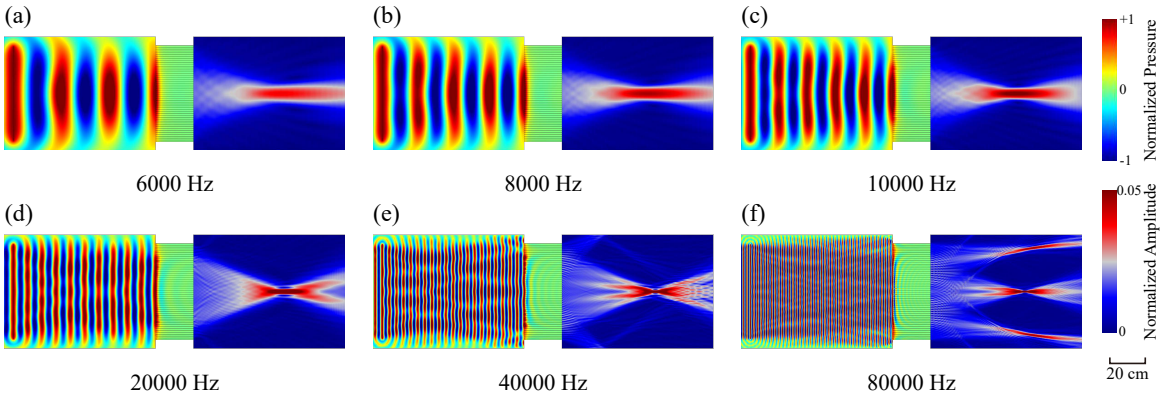

FIG. 7: A lens designed by spatial-gauge cooperative transformation theory for the water-air interface. Response to plane wave excitation is shown at (a) 6000 Hz, (b) 8000 Hz, (c) 10000 Hz, (d) 20000 Hz, (e) 40000 Hz, and (f) 80000 Hz. The incident field on the left is depicted with the real part of the complex pressure. The transmission field on the right is depicted with the amplitude of the complex pressure.

Then, the phase difference supplied by the lens is

$$\begin{aligned}\Delta\phi\left(y'\right) &= k_1\left(\frac{k_0'}{k_0}\left(\sqrt{y'^2+l_0^2}-l_0\right)+C_0/k_0\right)\\ &= k_1'\left(\sqrt{y'^2+l_0^2}-l_0\right)+C_1. \end{aligned} \tag{53}$$

It is thus clear that the designed lens is achromatic.

We set $x_1 = x_1' = -10$ cm, $x_2 = x_2' = 10$ cm, $l_0 = 50$ cm and $C_0 = 0$, from which the expression for $\hat{x_2}$ can be uniquely determined. 51 units with a width of 9.5 mm are arranged evenly along the y-axis and are separated by rigid walls with a thickness of 0.5 mm. Each unit has its corresponding $\hat{x_2}$, which can be obtained by substituting the ordinate of its center point into Eq. (52). Their interior is filled with the Willis-like material whose parameters are obtained by substituting $\hat{x_2}$ and Eqs. (46-48) into Eqs. (37-39). Detailed metamaterial parameters are given in Appendix B. The incident field and the transmission regions are set as two rectangular regions with a width of 80 cm and a height of 60 cm. Perfectly matched layers with a thickness of 10 cm surround both domains to avoid reflection on the external boundaries(not drawn for simplicity). A plane sound wave is excited by a line source with a length of 50 cm, placed 75 cm away from the left side of the metasurface.

Numerical simulation of the operation of the lens is reported in Fig. 7 for 6 different frequencies. A wave is incident from the water side. When it reaches the metasurface, only minor reflection occurs. Waves are transmitted through the Willis-like materials filling the unit cells composing the metasurface and are focused in air. The transmitted beams focus at a distance of about 50 cm after the metasurface. The focus is stable under a considerably broad frequency range, from 6000 Hz to 40000 Hz, validating achromaticity. The transmission field seems no longer ideal when it reaches 80000 Hz. This is mainly because

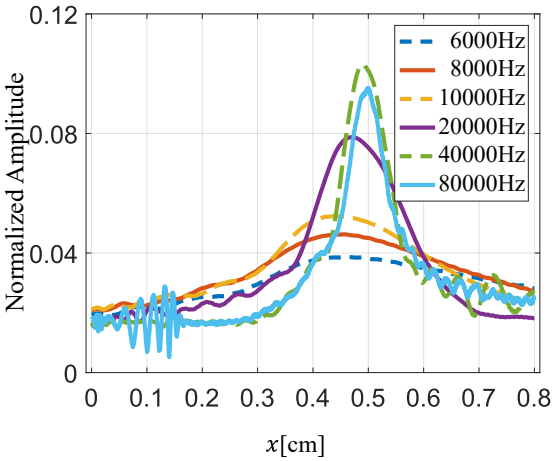

FIG. 8: Normalized pressure distribution on the transmission side of the metasurface along the $y = 0$ axis at different frequencies.

the sound wavelength on the air side decreases to about 4 mm, which is less than the thickness of the unit cell. Sound pressure distributions are shown along the horizontal axis $y = 0$ in Fig. 8. The lens performance appears to improve with increasing frequency. Actually, the acoustic wavelength decreases with frequency, causing waves to converge to a tighter focus. The pressure at the focal point exceeds by least 2-7 times the theoretical limit for plane wave transmission, $[|p_2/p_1| = 1/60$ in Eq. (28)]. However, the performance is not ideal only at 80000 Hz. Considering that the unit cell thickness may play an important role in practical design, a discussion of the relationship between thickness and broadband operation is provided in Appendix D.

III. CONCLUSION

In this paper, transformation acoustics has been considered from the perspective of broadband transmedia transmission with achromatic focusing for water-air acoustic communication. The spatial transformation and the gauge transformation were applied both separately and jointly in the design of transformation metamaterials. Reflectionless sound wave transmission between arbitrary different media can be achieved in 2D based on a spatial transformation. Transmitted waves own a conserved amplitude and can be steered with an arbitrary transmission angle. Gauge transformation was then introduced into transformation acoustics to provide a 1D solution. Perfect connection between media with very different acoustic impedances is achieved through Willis-like materials. Combining the two transformations, the dilemma of phase locking on the water-air interface can be effectively solved based on a spatial-gauge cooperative transformation. A focusing lens was designed for further enhancement of acoustic signals and was shown to provide broadband and achromatic operation. It should be mentioned that the designed metamaterials may be put into practice by applying the effective medium theory or homogenization. The operating bandwidth may degrade to some extent when involving resonance. However, the transformation proposed in this work leaves great flexibility in design parameters. Properly designed transformation function is conducive to the implementation of the designed metasurface. Subsequent study will be devoted to developing effective gradient Willis materials for better practicability of spatial-gauge cooperative transformation. The work in this paper is expected to provide theoretical support for transmedia acoustic communication and the development of additional application scenarios for transformation acoustics.

Acknowledgments

The authors acknowledge financial support by the National Natural Science Foundation of China 12072223, 12122207, 12021002 and 11991032). V.L. acknowledges financial support by the EIPHI Graduate School (ANR-17-EURE-0002).

Appendix A: Expression of matrix F_3

Equations (8a-8d) imply that $a^2+b^2 = c^2+d^2 = \alpha\beta \neq 0$. Multiplying Eq. (8c) with a and using Eq. (8b) implies $\alpha d = a$. Similarly, multiplying Eq. (8c) with c and using Eq. (8b) implies $\alpha b = -c$.

Inserting those relations in Eq. (8b) gives $(\alpha^2 - 1)bd = 0$. Hence, either of the three factors must equal zero. If $b = 0$, then $c = 0$ and $a^2 = d^2$; we are then led to $\alpha^2 = 1$. If $d = 0$, then $a = 0$ and $b^2 = c^2$; we are again led to $\alpha^2 = 1$. As a whole, $\alpha^2 = 1$ necessarily applies. Considering positive mass densities, $\alpha = 1$. As a result, solutions are of the form of Eq. (9).

Appendix B: Explicit expressions of material parameter

The metamaterials for the simulations in Sect. II A are described by

$$\begin{aligned}\rho'^{-1} &= \rho^{-1}\frac{FF^T}{J} \\ &= \frac{\rho^{-1}}{\frac{\partial x'}{\partial x}\frac{\partial y'}{\partial x} - \frac{\partial x'}{\partial y}\frac{\partial y'}{\partial x}}\begin{bmatrix} \frac{\partial x'}{\partial x}\frac{\partial x'}{\partial x} + \frac{\partial x'}{\partial y}\frac{\partial x'}{\partial y} & \frac{\partial x'}{\partial x}\frac{\partial y'}{\partial x} + \frac{\partial x'}{\partial y}\frac{\partial y'}{\partial y} \\ \frac{\partial y'}{\partial x}\frac{\partial x'}{\partial x} + \frac{\partial y'}{\partial y}\frac{\partial x'}{\partial y} & \frac{\partial y'}{\partial x}\frac{\partial y'}{\partial x} + \frac{\partial y'}{\partial y}\frac{\partial y'}{\partial y} \end{bmatrix}\end{aligned} \tag{B1}$$

$$K'^{-1} = \frac{K^{-1}}{\frac{\partial x'}{\partial x}\frac{\partial y'}{\partial x} - \frac{\partial x'}{\partial y}\frac{\partial y'}{\partial x}}, \tag{B2}$$

where the partial derivatives can be determined by Eq. (15) as

$$\begin{cases} \frac{\partial x'}{\partial x} = 1 + \frac{\sqrt{\beta - a_0^2}}{w_m}y, \\ \frac{\partial x'}{\partial y} = \frac{\sqrt{\beta - a_0^2}}{2} + \frac{\sqrt{\beta - a_0^2}}{w_m}x, \\ \frac{\partial y'}{\partial x} = -\frac{1-a_0}{w_m}y, \\ \frac{\partial y'}{\partial y} = \frac{a_0+1}{2} - \frac{1-a_0}{w_m}x. \end{cases} \tag{B3}$$

According to the discussion at the beginning of Sect. II, all parameters should be described by transformed coordinates. It can be noted that Eq. (15) is monotonic when $(x \in [-w_m/2, w_m/2] \cap y \in [-h_m/2, h_m/2])$. Then its inverse function can be given as

$$x=\frac{\left(\frac{a_0+1}{2}-\frac{\sqrt{\beta-a_0^2}}{w_m}y'+\frac{1-a_0}{w_m}x'\right)+\sqrt{\left(\frac{a_0+1}{2}+\frac{\sqrt{\beta-a_0^2}}{w_m}y'+\frac{1-a_0}{w_m}x'\right)^2+\frac{4(1-a_0)}{w_m}\left(\frac{\sqrt{\beta-a_0^2}}{2}y'-\frac{a_0+1}{2}x'\right)}}{\frac{2(1-a_0)}{w_m}},\tag{B4}$$

$$y=\frac{\left(-\frac{a_0+1}{2}+\frac{1-a_0}{w_m}x'+\frac{\sqrt{\beta-a_0^2}}{w_m}y'\right)+\sqrt{\left(-\frac{a_0+1}{2}+\frac{1-a_0}{w_m}x'+\frac{\sqrt{\beta-a_0^2}}{w_m}y'\right)^2+4\left(\frac{\sqrt{\beta-a_0^2}}{2}\frac{1-a_0}{w_m}+\frac{\sqrt{\beta-a_0^2}}{w_m}\frac{a_0+1}{2}\right)y'}}{2\left(\frac{\sqrt{\beta-a_0^2}}{2}\frac{1-a_0}{w_m}+\frac{\sqrt{\beta-a_0^2}}{w_m}\frac{a_0+1}{2}\right)}.\tag{B5}$$

Substituting them back to Eqs. (B1-B2), the required material parameters can then be acquired.

The metamaterials for the simulations in Sect. II B are described by

$$\begin{cases} S(x)=\frac{G(x)}{\rho}\frac{\partial G(x)}{\partial x}, \\ E(x)=\frac{1}{\rho}\left(\frac{\partial G(x)}{\partial x}\right)^2, \\ \rho''(x)=\frac{\rho}{G^2(x)}, \\ K''(x)=\frac{K}{G^2(x)}. \end{cases}\tag{B6}$$

Substituting Eqs. (29) and (34) into them, their explicit expression can be obtained

$$\begin{cases} S(x)=\frac{\left(a_0+a_1x+a_2x^2+a_3x^3\right)\left(a_1+2a_2x+3a_3x^2\right)}{\rho}, \\ E(x)=\frac{\left(a_1+2a_2x+3a_3x^2\right)^2}{\rho}, \\ \rho''(x)=\frac{\rho}{\left(a_0+a_1x+a_2x^2+a_3x^3\right)^2}, \\ K''(x)=\frac{K}{\left(a_0+a_1x+a_2x^2+a_3x^3\right)^2}. \end{cases}\tag{B7}$$

Similarly, the metamaterials for the simulations in Sect. II C are described by

$$\begin{cases} S'=\frac{G(x')}{\rho}\frac{\partial x'}{\partial x}\frac{\partial G(x')}{\partial x'}, \\ E'=\frac{1}{\rho}\frac{\partial x'}{\partial x}\left(\frac{\partial G(x')}{\partial x}\right)^2, \\ \rho'''(x')=\frac{\rho}{G^2(x')\frac{\partial x'}{\partial x}}, \\ K'''(x')=\frac{K}{G^2(x')}\frac{\partial x'}{\partial x}. \end{cases}\tag{B8}$$

Substituting Eqs. (47) and (48) into them, their explicit expression can be obtained

$$\begin{cases} S'=\frac{\left(a_0+a_1x'+a_2x'^2+a_3x'^3\right)\left(a_1x+2a_2x'+3a_3x'^2\right)}{\rho}\frac{F_3\hat{x_2}(y')-x_1+h_x}{\hat{x_2}(y')-x_1}, \\ E'=\frac{\left(a_1x+2a_2x'+3a_3x'^2\right)^2}{\rho}\frac{F_3\hat{x_2}(y')-x_1+h_x}{\hat{x_2}(y')-x_1}, \\ \rho'''(x')=\frac{\rho}{\left(a_0+a_1x'+a_2x'^2+a_3x'^3\right)^2\frac{F_3\hat{x_2}(y')-x_1+h_x}{\hat{x_2}(y')-x_1}}, \\ K'''(x')=\frac{K}{\left(a_0+a_1x'+a_2x'^2+a_3x'^3\right)^2}\frac{F_3\hat{x_2}(y')-x_1+h_x}{\hat{x_2}(y')-x_1}. \end{cases}\tag{B9}$$

where the explicit expression for $\hat{x_2}(y')$ is given in Eq. (52) and h_x is determined by

$$h_x=t_0+x_1-F_3x_2.\tag{B10}$$

Appendix C: Contribution of Willis coupling in transmedia acoustic transmission

The metamaterials defined by Eqs. (37-39) enable acoustic connection between arbitrarily different media. They would simplify to graded impedance-matching materials if Willis terms were removed. Here, we use an example to discuss the role of Willis coupling in transmedia transmission. We set $x_1=x_1'$ and $x_2=x_2'$ in Eq. (B9) whereas other parameters are set following Sect. II. B. Then the transformation-induced metamaterial can be determined with parameters consistent with Fig. 6(f-g). The graded material used for comparison is set to have the same mass density and bulk modulus but with $S'=0$ and $E'=0$. Power flow transmittance is defined as $T=\frac{|p_t^2|/Za}{|p_i^2|/Zw}$ where $p_i=1$ is the unitary incident amplitude in water and p_t is the transmission amplitude in air, respectively. The simulation results for the two designs in the range 5 kHz-40 kHz are presented in Fig. 9. The blue line represents the transformation-induced metamaterial, exhibiting perfect performance. When the Willis terms are removed, transmittance changes to the orange line. Almost no power flow is transmitted at lower frequencies, whereas the transmittance gradually approaches 1 as the frequency increases.

It can be concluded that Willis coupling compensates for the reflections caused by drastic impedance changes. In the homogeneization picture, the graded material can be regarded as a thin layer at lower frequencies, for which the wavelength is relatively large, thus providing an abrupt impedance change that converges to a step function for the zero frequency. For a large frequency, impedance changes slow down compared to the shorter wavelength. The contribution of the Willis terms thus diminishes and the transmittance provided by the two designs almost overlap. As a consequence, a slower impedance change rate provides a lower operating frequency for graded materials without Willis coupling. Conversely, a graded

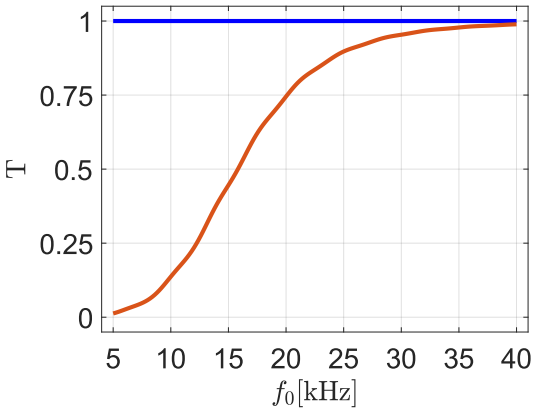

FIG. 9: Comparison of the transmittance provided by metamaterials with Willis coupling (blue line) and graded material.

material incorporating Willis coupling achieves broad bandwidth transmedia transmission compactly. However, it should be mentioned that the transformation function in this work, as well as the grading function, are presented as polynomials, whereas the definition of transformation $\mathcal{F}_2$ is actually not unique. There may still be a specific transformation function that leads to a slighter difference between metamaterial and graded material transmittance at lower frequencies. Hence the contribution of Willis terms can be mitigated and the design of the metamaterial may be simplified.

Appendix D: Effect of the unit thickness on the achromatic lens

Simulation results for generalized Snell's law based lenses with different thicknesses of units at three different frequencies 6000 Hz, 10000 Hz, and 40000 Hz, are shown in Fig. 10. Three designs were examined, including 25 units with a thickness of 1.95 cm, 13 units with a thickness of 3.95 cm, and 7 units with a thickness of 7.95 cm. All units are separated by rigid walls with a thickness of 0.5 mm. Other configurations are consistent with those in Sect. II C.

It can be observed that the lens with 25 discrete units operates normally at low frequencies (6000 Hz in Fig. 10 (a) and 10000 Hz in Fig. 10 (b)). However, a failure similar to Fig. 7 (f) also occurs at 40000 Hz. The performance at low frequency is basically the same when the number of units decreases to 13 in Fig. 10 (d), while some additional scattering occurs in the transmission field at 10000 Hz in Fig. 10 (e). This lens does not work at all at 40000 Hz in Fig. 10 (f). When the number of units decreased to 7, the convergence of the sound beam is still observed at 6000 Hz as shown in Fig. 10 (g). Interestingly, the performance at 10000 Hz in Fig. 10 (h) can be barely maintained as well even though the wavelength decreases to 34 mm, which is less than half of the unit thickness. This could be greatly beneficial for the production of metamaterials in practice. Substantially, almost no reflection on the water side can be perceived in all cases even in Fig. 10 (i).

* Electronic address: wangyanfeng@tju.edu.cn

[1] Oleg A Godin. Sound transmission through water–air interfaces: New insights into an old problem. *Contemporary Physics*, 49(2):105–123, 2008.

[2] Tie Qiu, Zhao Zhao, Tong Zhang, Chen Chen, and CL Philip Chen. Underwater internet of things in smart ocean: System architecture and open issues. *IEEE transactions on industrial informatics*, 16(7):4297–4307, 2019.

[3] Zhi Sun, Hongzhi Guo, and Ian F Akyildiz. High-data-rate long-range underwater communications via acoustic reconfigurable intelligent surfaces. *IEEE Communications Magazine*, 60(10):96–102, 2022.

[4] Timothy G Leighton. How can humans, in air, hear sound generated underwater (and can goldfish hear their owners talking)? *The Journal of the Acoustical Society of America*, 131(3):2539–2542, 2012.

[5] Allan D Pierce. *Acoustics: an introduction to its physical principles and applications*. Springer, 2019.

[6] Oleg A Godin. Anomalous transparency of water-air interface for low-frequency sound. *Physical Review Letters*, 97(16):164301, 2006.

[7] OA Godin. Transmission of low-frequency sound through the water-to-air interface. *Acoustical Physics*, 53:305–312, 2007.

[8] Oleg A Godin. Low-frequency sound transmission through a gas–liquid interface. *The Journal of the Acoustical Society of America*, 123(4):1866–1879, 2008.

[9] Alice Bretagne, Arnaud Tourin, and Valentin Leroy. Enhanced and reduced transmission of acoustic waves with bubble meta-screens. *Applied Physics Letters*, 99(22):221906, 2011.

[10] Zheren Cai, Shengdong Zhao, Zhandong Huang, Zheng Li, Meng Su, Zeying Zhang, Zhipeng Zhao, Xiaotian Hu, Yue-Sheng Wang, and Yanlin Song. Bubble architectures for locally resonant acoustic metamaterials. *Advanced Functional Materials*, 29(51):1906984, 2019.

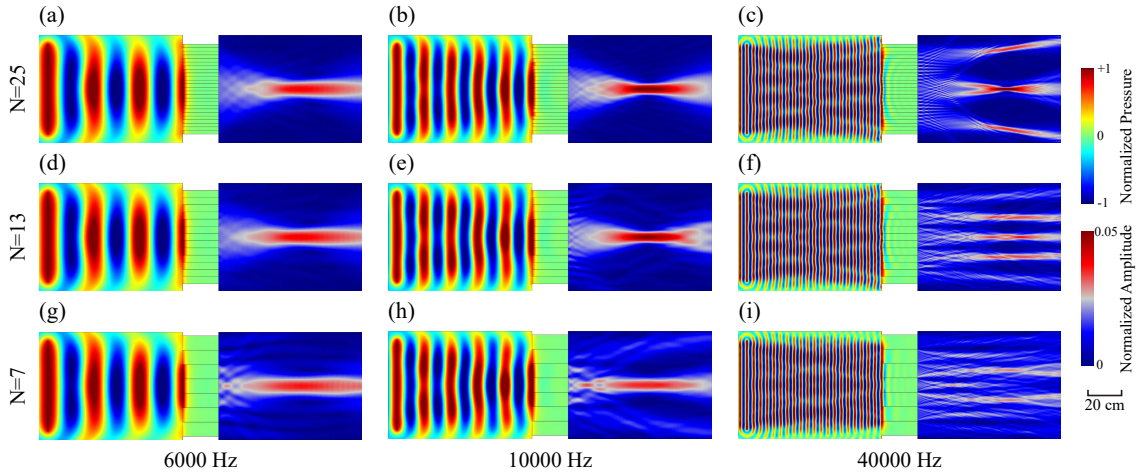

FIG. 10: The comparison of lenses with different numbers of units designed by spatial-gauge cooperative transformation theory for the water-air interface. The performance of the lens discretized into 25 units with a thickness of 1.95cm at (a) 6000 Hz, (b) 10000 Hz, (c) 40000 Hz. The performance of the lens discretized into 13 units with a thickness of 3.95cm at (d) 6000 Hz, (e) 10000 Hz, (f) 40000 Hz. The performance of the lens discretized into 7 units with a thickness of 7.95cm at (g) 6000 Hz, (h) 10000 Hz, (i) 40000 Hz. The incident field on the left is depicted with the real part of the complex pressure. The transmission field on the right is depicted with the amplitude of the complex pressure.

[11] Yan-Feng Wang, Yi-Ze Wang, Bin Wu, Weiqiu Chen, and Yue-Sheng Wang. Tunable and active phononic crystals and metamaterials. *Applied Mechanics Reviews*, 72(4):040801, 2020.

[12] Badreddine Assouar, Bin Liang, Ying Wu, Yong Li, Jian-Chun Cheng, and Yun Jing. Acoustic metasurfaces. *Nature Reviews Materials*, 3(12):460–472, 2018.

[13] Xiao-Tong Gong, Hong-Tao Zhou, Shao-Cong Zhang, Yan-Feng Wang, and Yue-Sheng Wang. Tunable sound transmission through water–air interface by membrane-sealed bubble metasurface. *Applied Physics Letters*, 123(23):231703, 12 2023.

[14] Zhandong Huang, Shengdong Zhao, Yiyuan Zhang, Zheren Cai, Zheng Li, Junfeng Xiao, Meng Su, Qiuquan Guo, Chuanzeng Zhang, Yaozong Pan, et al. Tunable fluid-type metasurface for wide-angle and multifrequency water-air acoustic transmission. *Research*, 2021, 2021.

[15] Taehwa Lee and Hideo Iizuka. Sound propagation across the air/water interface by a critically coupled resonant bubble. *Physical Review B*, 102(10):104105, 2020.

[16] Hui Zhang, Zhi Wei, Li Fan, Jianmin Qu, and Shu-yi Zhang. Tunable sound transmission at an impedance-mismatched fluidic interface assisted by a composite waveguide. *Scientific Reports*, 6(1):34688, 2016.

[17] Eun Bok, Jong Jin Park, Haejin Choi, Chung Kyu Han, Oliver B Wright, and Sam H Lee. Metasurface for water-to-air sound transmission. *Physical Review Letters*, 120(4):044302, 2018.

[18] Xin-Rui Li, Yu-Rou Jia, Yan-Chun Luo, Jie Yao, and Da-Jian Wu. Mixed focused-acoustic-vortices generated by an artificial structure plate engraved with discrete rectangular holes. *Applied Physics Letters*, 118(4), 2021.

[19] Chengzhi Shi, Marc Dubois, Yuan Wang, and Xiang Zhang. High-speed acoustic communication by multiplexing orbital angular momentum. *Proceedings of the National Academy of Sciences*, 114(28):7250–7253, 2017.

[20] Shao-Cong Zhang, Hong-Tao Zhou, Xiao-Tong Gong, Yan-Feng Wang, and Yue-Sheng Wang. Discrete metasurface for extreme sound transmission through water-air interface. *Journal of Sound and Vibration*, 575:118269, 2024.

[21] Bogdan-Ioan Popa. Broadband sound pressure enhancement in passive metafluids. *Physical Review B*, 96(9):094305, 2017.

[22] Ping Zhou, Han Jia, Yafeng Bi, Yunhan Yang, Yuzhen Yang, Peng Zhang, and Jun Yang. Water–air acoustic communication based on broadband impedance matching. *Applied Physics Letters*, 123(19):191701, 2023.

[23] Peder C Pedersen, Oleh Tretiak, and Ping He. Impedance-matching properties of an inhomogeneous matching layer with continuously changing acoustic impedance. *The Journal of the Acoustical Society of America*, 72(2):327–336, 1982.

[24] Hong-Tao Zhou, Shao-Cong Zhang, Tong Zhu, Yu-Ze Tian, Yan-Feng Wang, and Yue-Sheng Wang. Hybrid metasurfaces for perfect transmission and customized manipulation of sound across water–air interface. *Advanced Science*, 10(19):2207181, 2023.

[25] Jingjing Liu, Zhengwei Li, Bin Liang, Jian-Chun Cheng, and Andrea Alù. Remote water-to-air eavesdropping with a phase-engineered impedance matching metasurface. *Advanced Materials*, page 2301799, 2023.

[26] Huanyang Chen and Che Ting Chan. Acoustic cloaking and transformation acoustics. *Journal of Physics D: Applied Physics*, 43(11):113001, 2010.

[27] Zeren Zhang, Liujun Xu, Teng Qu, Min Lei, Zhi-Kang Lin, Xiaoping Ouyang, Jian-Hua Jiang, and Jiping Huang. Diffusion metamaterials. *Nature Reviews Physics*, 5(4):218–235, 2023.

[28] John B Pendry, David Schurig, and David R

Smith. Controlling electromagnetic fields. *Science*, 312(5781):1780–1782, 2006.

[29] Ulf Leonhardt. Optical conformal mapping. *Science*, 312(5781):1777–1780, 2006.

[30] Steven A Cummer and David Schurig. One path to acoustic cloaking. *New Journal of Physics*, 9(3):45, 2007.

[31] Huanyang Chen and Che Ting Chan. Acoustic cloaking in three dimensions using acoustic metamaterials. *Applied Physics Letters*, 91(18):183518, 2007.

[32] Steven A Cummer, Bogdan-Ioan Popa, David Schurig, David R Smith, John Pendry, Marco Rahm, and Anthony Starr. Scattering theory derivation of a 3d acoustic cloaking shell. *Physical Review Letters*, 100(2):024301, 2008.

[33] Andrew N Norris. Acoustic cloaking theory. *Proceedings of the Royal Society A: Mathematical, Physical and Engineering Sciences*, 464(2097):2411–2434, 2008.

[34] Peter A Kerrian, Amanda D Hanford, Dean E Capone, and Benjamin S Beck. Development of a perforated plate underwater acoustic ground cloak. *The Journal of the Acoustical Society of America*, 146(4):2303–2308, 2019.

[35] Mohamed Farhat, Sebastien Guenneau, Stefan Enoch, and Alexander B Movchan. Cloaking bending waves propagating in thin elastic plates. *Physical Review B*, 79(3):033102, 2009.

[36] Ahmad Zareei and Mohammad-Reza Alam. Broadband cloaking of flexural waves. *Physical Review E*, 95(6):063002, 2017.

[37] Graeme W Milton, Marc Briane, and John R Willis. On cloaking for elasticity and physical equations with a transformation invariant form. *New Journal of Physics*, 8(10):248, 2006.

[38] Michele Brun, Sébastien Guenneau, and Alexander B Movchan. Achieving control of in-plane elastic waves. *Applied Physics Letters*, 94(6):061903, 2009.

[39] CZ Fan, Y Gao, and JP Huang. Shaped graded materials with an apparent negative thermal conductivity. *Applied Physics Letters*, 92(25):251907, 2008.

[40] Qingxiang Ji, Xueyan Chen, Jun Liang, Vincent Laude, Sébastien Guenneau, Guodong Fang, and Muamer Kadic. Non-singular homogeneous polyhedral heat cloak and its realization. *ES Energy & Environment*, 7:29–39, 2019.

[41] Guoqiang Xu, Kaichen Dong, Ying Li, Huagen Li, Kaipeng Liu, Longqiu Li, Junqiao Wu, and Cheng-Wei Qiu. Tunable analog thermal material. *Nature communications*, 11(1):6028, 2020.

[42] JY Li, Yutang Gao, and JP Huang. A bifunctional cloak using transformation media. *Journal of Applied Physics*, 108(7):074504, 2010.

[43] Troy Stedman and Lilia M Woods. Cloaking of thermoelectric transport. *Scientific Reports*, 7(1):6988, 2017.

[44] Yu-Ze Tian, Yan-Feng Wang, Gan-Yun Huang, Vincent Laude, and Yue-Sheng Wang. Dual-function thermoelastic cloak based on coordinate transformation theory. *International Journal of Heat and Mass Transfer*, 195:123128, 2022.

[45] Allan Greenleaf, Matti Lassas, and Gunther Uhlmann. On nonuniqueness for calderon's inverse problem. *arXiv preprint math/0302258*, 2003.

[46] Romain Fleury, Francesco Monticone, and Andrea Alù. Invisibility and cloaking: Origins, present, and future perspectives. *Physical Review Applied*, 4(3):037001, 2015.

[47] Yongquan Liu, Zhaoyang Ma, and Xianyue Su. Linear transformation method to control flexural waves in thin plates. *The Journal of the Acoustical Society of America*, 140(2):1154–1161, 2016.

[48] Yaolu Liu, Houbo Li, Jun Zhang, Xuyang Liu, Liangke Wu, Huiming Ning, and Ning Hu. Design of elastic metasurfaces for controlling shear vertical waves using uniaxial scaling transformation method. *International Journal of Mechanical Sciences*, 169:105335, 2020.

[49] Andrew N Norris and Alexander L Shuvalov. Elastic cloaking theory. *Wave Motion*, 48(6):525–538, 2011.

[50] John R Willis. Variational principles for dynamic problems for inhomogeneous elastic media. *Wave Motion*, 3(1):1–11, 1981.

[51] Li Quan, Younes Ra'di, Dimitrios L Sounas, and Andrea Alù. Maximum willis coupling in acoustic scatterers. *Physical review letters*, 120(25):254301, 2018.

[52] Shu-Yan Zhang, Dong-Jia Yan, Yue-Sheng Wang, Yan-Feng Wang, and Vincent Laude. Wave propagation in one-dimensional fluid-saturated porous phononic crystals with partial-open pore interfaces. *International Journal of Mechanical Sciences*, 195:106227, 2021.

[53] Choonlae Cho, Xinhua Wen, Namkyoo Park, and Jensen Li. Acoustic willis meta-atom beyond the bounds of passivity and reciprocity. *Communications Physics*, 4(1):82, 2021.

[54] Hervé Lissek, Etienne Rivet, Thomas Laurence, and Romain Fleury. Toward wideband steerable acoustic metasurfaces with arrays of active electroacoustic resonators. *Journal of Applied Physics*, 123(9), 2018.

[55] Ali Zabihi, Chadi Ellouzi, and Chen Shen. Tunable, reconfigurable, and programmable acoustic metasurfaces: A review. *Frontiers in Materials*, 10:1132585, 2023.